Field Quality and Fabrication Analysis of HQ02 Reconstructed Nb_3Sn Coil Cross Sections

E.F. Holik, G. Ambrosio, A. Carbonara, D.R. Dietderich, J. Dimarco, I. Pong, G.L. Sabbi, C. Santini, J. Schmalzle, X. Wang

***Abstract*— The US LHC Accelerator Research Program (LARP) quadrupole HQ02 was designed and fully tested as part of the low-beta quad development for Hi-Lumi LHC. HQ02's design is well documented with full fabrication accounting along with full field analysis at low and high current. With this history, HQ02 is an excellent test bed for developing a methodology for measuring turn locations from magnet cross sections and comparing with CAD models and measured field. All 4 coils of HQ02 were cut in identical locations along the magnetic length corresponding to magnetic field measurement and coil metrology. A real-time camera and coordinate measuring equipment was used to plot turn corners. Measurements include systematic and random displacements of winding blocks and individual turns along the magnetic length. The range of cable shifts and the field harmonic range along the length are in agreement, although correlating turn locations and measured harmonics in each cross section is challenging.**

***Index Terms*— Accelerator Magnets, IR Quadrupoles, Magnet analysis techniques.**

I. Introduction

The Hi-Lumi LHC upgrade requires ultra-high performance Nb_3Sn quadrupoles for focusing the beam at collision points. The integrated luminosity of the LHC is slated to increase by a factor of 10 by the end of the project in 2025 [1]. High-performance Nb_3Sn final-focusing, Interaction Region (IR) quadrupoles are one of the enabling technology for the luminosity upgrade. These 150-mm-aperture quadrupoles have stringent field quality requirements to maximize the instantaneous luminosity and minimize beam loss [2]. With this in mind, several studies have sought to understand the origin of field quality aberrations at the coil level for both dipoles [3-5] and focusing quadrupoles [6-7]. The majority of previous work sought to determine conductor and component misalignment based on measured field quality for multiple magnets [3-7]. This work attempts to link the field quality of a single magnet with measured turn displacements from coil cross sections. This link will be shown in two broad steps: first to quantify turn location and turn movement with respect to nominal and then determine expected magnet field variance and quality in HQ02 based on turn location. LARP has been gradually developing IR quadrupoles for Hi-Lumi LHC since 2004 [8]. HQ02 was an intermediate generation magnet with 120-mm-aperture to test several aspects of superconducting quadrupole construction and operation [9-11]. The magnetic field harmonics of HQ02 were measured along the length of the magnet after magnet assembly and at full field in preparation for Hi-Lumi LHC [12-13]. Afterwards, all 4 coils of the magnet were cut at specific locations along the length coinciding with magnetic field measurements. Ultimately the measured field quality during magnet testing will be compared to the calculated field quality from magnet cross sections.

The work of E. F. Holik was supported by the Toohig Fellowship in Accelerator Science from the US LHC Accelerator Research Program. This work was supported by the US Department of Energy through the US LHC Accelerator Research Program (LARP) and by the High Luminosity LHC Project at CERN.

E. F. Holik, is with Angelo State University, San Angelo, TX, 76904 USA and Fermi National Accelerator Laboratory, Batavia, IL 60510 USA (e-mail: eholik@fnal.gov).

G. Ambrosio, A. Carbonara, and C. Santini are with the Fermi National Accelerator Laboratory, Batavia, IL 60510 USA

J. Schmalzle is with Brookhaven National Laboratory, Upton, NY 11973 USA.

D. R. Dietderich, I. Pong, G. L. Sabbi, and X. Wang are with the Lawrence Berkeley National Laboratory, Berkley, CA 94720 USA.

II. HQ02 Cross Section Data Collection

The magnet HQ02 was comprised of coils HQ15, HQ16, HQ17, and HQ20 [9]. All four coils are nominally the same design and size. HQ17 had braided-on type cable insulation while the other three had sock type insulation. Braided-on S2 glass insulation tends to constrict lateral growth during heat treatment and reduce the length contraction of conductor during heat treatment [14]. Coil HQ17 was thus analyzed independently of the other three coils.

A. Cross Section Sample preparation

The locations of each cut is indicated by dotted lines in Fig. 1. The a_3 and b_3 harmonics are also plotted for comparison. All coils were sufficiently labeled to completely orient each segment after cutting. The labeling scheme is also presented in Fig. 1. All coils were water jet cut at BNL. All data was collected using an optical comparator at FNAL made by Optical Gauging Products, which can measure and store the position of points on a plane with a systematic error standard deviation less than three μm. The flexibility of the optical comparator allowed cross sections to be analyzed without polishing or extensive surface preparation.

B. Turn Location Measurement

The four corners of each turn were collected as points. A digital protractor was used to identify each corner in the following way: first, pushing one line to be tangent to the longer edge of the cable and then without rotation, the protractor was shifted until the second line was tangent to one strand of the shorter edge. In this process, some issues were encountered due to: not perfect alignment of strands, not perfectly sharp edge of strands, increased cable thickness at the second/third strand due to the Stainless Steel core, and

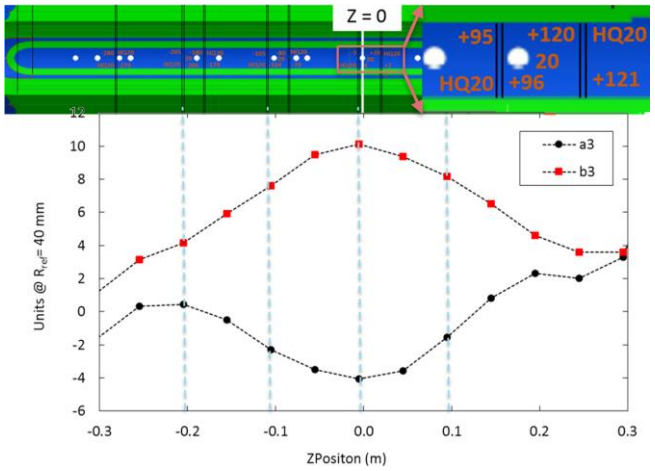

Fig. 1. Measured a3 and b3 (hexapole) harmonics measured along the length of HQ02 and corresponding locations where the internal coils were cut. The top right coil labeling scheme in mm completely orients each segment for cross section reassembly.

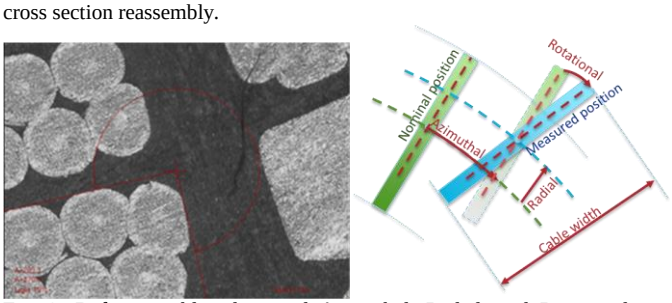

Fig. 2. Defining cable edges and Azimuthal, Radial, and Rotational turn displacements.

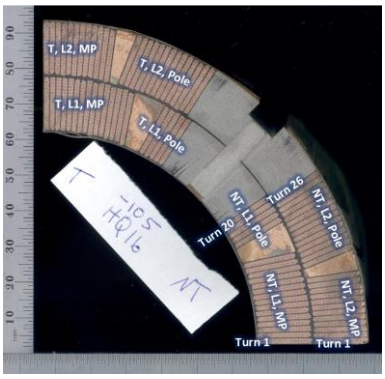

Fig. 3. Labeling scheme for HQ02 coil blocks.

varying strand triplets at some turn edges. The same cross section was measured multiple times with a Root-Mean-Square distance between each measurement of 12 µm. This value set the uncertainty of each measurement. An example of defining a cable edge is seen in Fig. 2.

C. Individual Cross Section Data Collection

The first attempt to define a coordinate system included determining the position of each turn relative to the coil outer diameter and the alignment keyway. Unfortunately, the outer coil surface proved too rough and non-repeatable to compare cross sections. To remove this variability, the cloud of collected points was best fit to the nominal position of each turn. In other words the cloud of points were translated and rotated until the RMS distance between measured and nominal turn position was minimized. In this manner all cross sections were analyzed by a repeatable and reliable process.

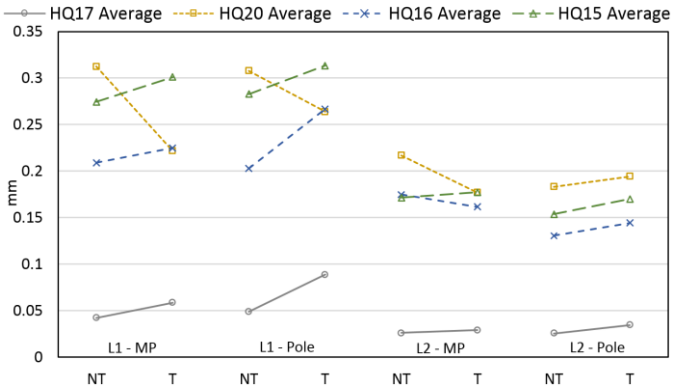

Fig. 4a. Block cable expansion with respect to measured pre-reaction width. The 2-sigma uncertainty for each data point is 43 µm. The NT and T data points are connected for easy observation of coil asymmetries.

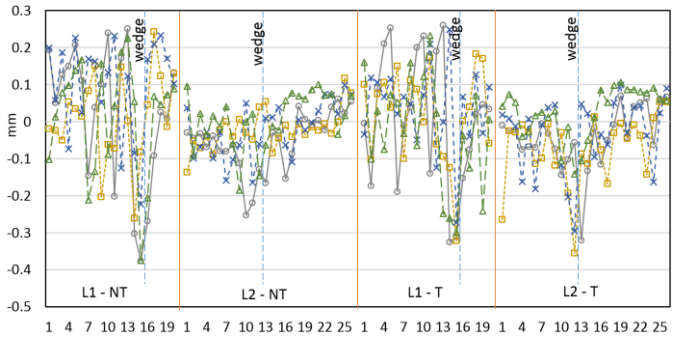

Fig. 4b. Radial turn position with respect to nominal. Layer separation and wedge location is indicated by vertical lines. Turn one for each layer is at the midplane. The two-sigma uncertainty for each data point is 55 µm.

D. Reassembled Collared Cross Section Data Collection

Three full cross section have been assembled using coils HQ17, HQ16, HQ15, HQ20 from the first quadrant counterclockwise. The four coils were assembled with four collars fastened together with ¼-20 bolts and tightened to 100 in-lbs of torque, the same value as coil pack assembly. The cross sections analyzed were at z = -5, -79, -105 mm as shown in Fig. 1.

The rationale for collecting data from a full collared cross section is five fold:

1. After being water jet cut, the coils tend to flair outward increasing the effective outer radius. The collars place the coils back into the original shape and outer radius;
2. By measuring actual cable positions for full cross sections all geometric systematic effects due to coil size, coil asymmetry, coil thickness, midplane offsets, tooling and component tolerance, etc. are accounted for.
3. The relative position of each coil is captured when fully assembled;
4. When using the collars, determining a coordinate system is independent of coil deformation and can be based on collar position rather than OD and keyway;
5. Furthermore, rigid motion of all 4 coils has minimal effect on calculated harmonics. For example, a full 1 mm translation produces less than one unit of any harmonic.

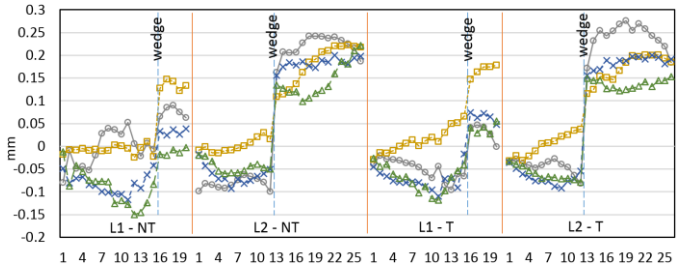

Fig. 5a. Average azimuthal turn position with respect to nominal. A positive value indicates a displacement toward the pole. The two-sigma uncertainty for each data point is 35 µm.

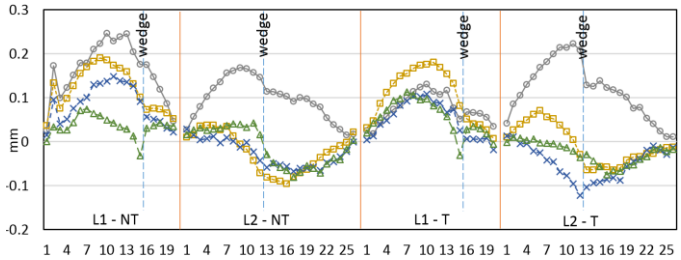

Fig. 5b. Average turn rotation with respect to nominal. A positive value indicates a displacement of the major edge toward the pole. The two-sigma uncertainty for each data point is 29 µm.

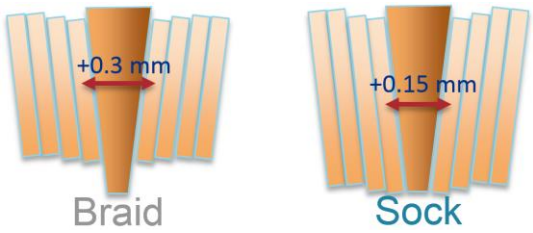

Fig. 6. Demonstration of how a narrower cable sits higher on the wedge and thus takes up more azimuthal space.

III. Turn Displacements

For each coil cross section, several data has been calculated: cable radial and azimuthal displacement with respect to the nominal cross section, cable width and expansion during heat treatment, and cable thickness as indicated in Fig. 2. Turns are divided into four blocks: the Transition/Non-Transition side and Layer 1/Layer 2 as indicated in Fig. 3. The different colors represent a different coil cross section, according to the legend.

A. Cable Width

Fig. 4a clearly shows the different level of expansion between coil HQ17 and the other coils. Coil HQ17 used cable with braided-on insulation while the other coils used cable with sock type insulation. The braided on insulation constricts the cable and reduces the expansion during heat treatment [9].

B. Conductor Alignment

Beginning with coil winding and ultimately for fully impregnated coils, all turns typically press against the outer surface of shell-type, cosine theta coils such as HQ02. Fig. 4b shows the average radial position of each turn with turn 1 starting at the midplane of each side. The outer, L2 coil has very little variation in radial position since it is pressing against the well-defined outer surface of the impregnation tooling. The inner L1 coil has much more variability since it is pressing against the less-defined interlayer insulation. The L1 and L2 radial standard deviation is 79 and 144 µm respectively.

C. Azimuthal Position and Rotation

In Fig. 5a there is a significant azimuthal shift near the wedge. The cause of this large wedge jump is likely 2-fold: additional insulation on each wedge on the order of 100 µm (125 µm nominal, 175 µm measured) and the reduced cable width expansion of HQ17 allowing cable to reside on the thicker outer part of the wedge as demonstrated in Fig. 6.

In Fig. 5b there is a clear rotational difference between HQ17 and the other coils. Having reduced cable width allows layer 2 turns to rotate with respect to nominal.

IV. Turn Waviness

Longitudinal waviness is defined as the amount that each turn or block shifts as a function of longitudinal position. More specifically, it is the difference in position of a block or turn as measured in two independent cross sections of a coil. In this manner the root mean square waviness for two cross sections that are only one mm apart should be approximately zero. The root-mean-square waviness for two cross sections that are several meters apart should asymptotically approach some value related to the constraints of the coil cavity. In this manner the measured harmonic standard deviations and

TABLE I
Displacements and Waviness for HQ02 Coils

		Braid (Coil 17)			Sock (Coils 15, 16, & 20)		
		Radial (µm)	Azimuthal (µm)	Rotation (µm)	Radial (µm)	Azimuthal (µm)	Rotation(µm)
Block RMS	Displacement from Nominal	59	125	118	67	111	67
	Displacement from Average	46	36	84	52	48	34
	Waviness 100 mm	41	5	27	30	16	16
	Waviness 200 mm	66	4	40	68	42	29
Turn RMS	Displacement from Nominal	156	138	131	127	114	80
	Displacement from Average	116	46	96	107	49	42
	Waviness 100 mm	90	11	29	92	20	16
	Waviness 200 mm	124	8	46	110	47	31
	Coil Cavity	1.5%	3.9%	-	1.6%	6.0%	-
	Cable Expansion	0.4%	4.4%	-	1.6%	3.8%	-
	Free Space	159 per layer	-7 per turn	-	0	28 per turn	-

RMS displacement, waviness, and free space of each turn and coil block. Analysis is based on 20 total cross sections. RMS Displacement is the displacement of each block or turn with respect to the nominal position and to the average position of all coils. Waviness is the RMS shift of each turn or block between cross sections 100 and 200 mm apart. The coil cavity is the value that the cable is allowed to expand into. The cable expansion is measured from cable expansion experiments and other cross sections. The free space is the difference between the cavity size and the cable expansion.

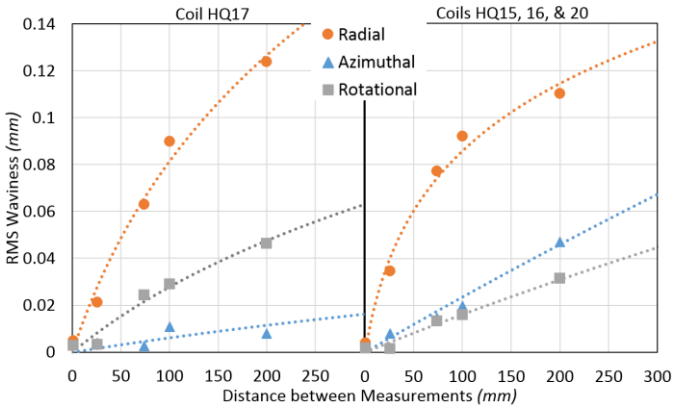

Fig. 7. Radial, Azimuthal, and Rotational waviness for HQ17 on the left and all other coils on the right.

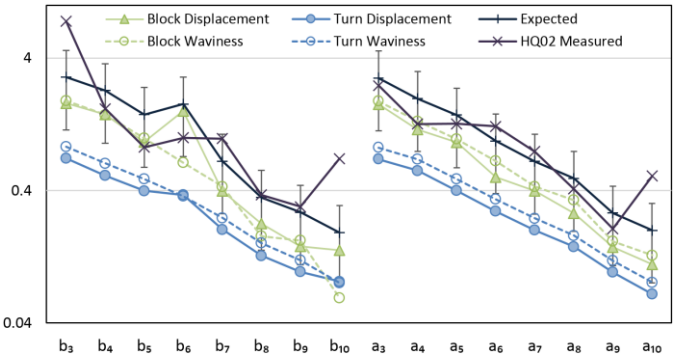

Fig. 8. RMS harmonics as measured and as calculated from the quadrature sum of block and turn displacement and waviness.

waviness should be directly correlated. Waviness does not account for systematic displacements or systematic harmonics but is accounted for by the measured displacements from nominal in the previous section. Data was collected from all four coils of HQ02, but HQ17 data was split from the others due to the difference in cable insulation.

The radial waviness in all coils is quite consistent despite HQ17 having roughly 159 µm per layer more radial free space compared to other coils. The bulk of this additional free space is realized by additional turn rotation waviness as seen in Fig. 7 for both the blocks and turns.

The azimuthal free space using sock type insulation is 28 µm per turn or 280 and 364 µm for L1 and L2 while the braid type insulation has zero free space. The braided on insulation is 104 µm thick and the sock type is 90 µm thick [10]. This differences produces the various coil cavity sizes seen in Table I. Sock type coil waviness is 5 times larger than the braided-on insulation of HQ17 as seen in Fig. 7. The azimuthal free space corresponds very well with azimuthal waviness. TABLE I provides a baseline for simulating the range of harmonics that should be measured longitudinally along the magnetic length.

V. Harmonics Based on Displacements and Waviness

The amount that each harmonic changes longitudinally is determined by how each coil, block, and turn moves laterally or shifts along the magnet. A Monte-Carlo code was written in Java to calculate the harmonics based on 36 line currents uniformly distributed within each cable block. The code neglects effects from iron. Random turn and block shifts are

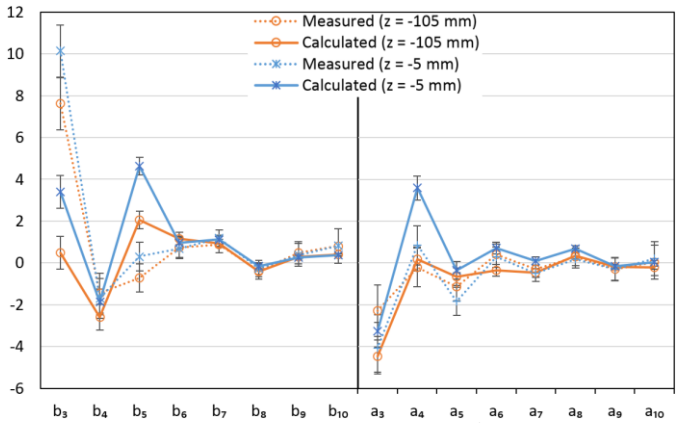

Fig. 9. Measured harmonics and calculated harmonics from coil cross sections at two specific locations in HQ02.

binomially distributed with a standard deviation based on cross sectional data in TABLE I.

The normal and skew RMS harmonics are presented in Fig. 8 as generated by displacements and waviness. The total expected RMS harmonics and the actual measured RMS harmonics are presented in Fig. 8 as well. The reader is reminded that $RMS^2 = \sigma^2 + avg^2$ for all values. The b_3, b_{10}, and a_{10} measured harmonics are significantly larger than expected based on cross section data. The b_{10} and a_{10} harmonics are likely due to probe resolution issues for high order harmonics. The b_3 harmonic is 2.7σ larger than what would be expected and suggests that the large b_3 in HQ02 is not from turn movement or waviness within the coils.

VI. Harmonics from Reconstructed Cross Sections

Cross sections from all four coils were reconstructed as close as possible to the actual HQ02 magnet at z = -5 mm and -105 mm. The shim package and torque specification was identical to what was used in HQ02.

All previous consideration apply to the process of collecting data points, except for the reference frame setting. Rather than using a best fit approach, the center of each keyway was computed and the center of the reference frame was set at the intersection of the line passing through opposite keyway centers.

The magnetic field was calculated using COMSOL with the iron properties equal to the magnetization chart used in OPERA. Various comparisons of COMSOL with OPERA and ROXIE were performed with indistinguishable results [11].

The measured and calculated harmonics are presented in Fig. 9. The measured harmonics are from a 100 mm long rotating coil. Calculated harmonics are from full magnet cross sections with uncertainties based on 100 mm waviness data. Measured harmonics vary little between z = -5 mm and z = -105 mm due to the smoothing, integral nature of the 100 mm rotating coil. The calculated field from single cross sections vary much more.

Large variability in a_4 indicates that the reconstructed cross sections have some oblong shape that usually is straightened with the full magnet structure. Thus a_4 variability is expected. The measured b_3 harmonic is 4.1σ larger than the reconstructed b_3 calculated harmonic. This is consistent to the

conclusion from RMS harmonic analysis. The large disagreement between measurement and calculation for b_3 indicates that either the combined uncertainty of turn measurement, loaded coil position, and measured harmonics is significantly larger than supposed or the b_3 harmonic is originating outside the coils of HQ02. All other harmonics such as a_3 and b_4 are in good agreement between measurement and calculation.

VII. Conclusion

Turn locations were measured at several cross sections of HQ02 by a coordinate measuring optical comparator. Conductor RMS displacement and waviness correlate well with RMS harmonics. The agreement between full reconstructed magnet cross sections and actual measured harmonics is not as strong. This is partly due to the measured harmonics being an average based on the length of the harmonic probe while the cross section is a point like assessment of turn position. The large b_3 harmonic is significantly larger than both RMS conductor displacements and reconstructed magnet cross sections suggest implying other sources of error in turn measurement or the particular harmonic originates outside the coils. The agreement for all other harmonics is good.

Acknowledgment

The authors would like to thank Jose Duran, Ethan Sprague, and DJ Warren for help with data collection and discussion. The author would also like to thank the QC department at Fermilab for the use of the optical comparator.

References

[1] "HL-LHC Preliminary Design Report", CERN-ACC-2014-0300, 28 November 2014.
[2] E. Todesco, *et al*., "Design studies for the low-beta quadrupoles for the LHC luminosity upgrade," *IEEE Trans. App. Supercond.*, vol. 23, no. 3, p. 4003305, June 2013.
[3] W. Scandale *et al*., "Influence of Mechanical Tolerances on Field Quality in the LHC Main Dipoles," *IEEE Trans. App. Supercond*, vol. 10, no. 1, pp. 73-76, March 2000.
[4] P. Ferracin, *et al.*, "Azimuthal coil size and field quality in the main CERN Large Hadron Collider dipoles," *Phys. Rev. ST Accel. Beams* vol. 5, 062401, June 2002.
[5] P. Ferracin, *et al.*, "Modeling of random geometric errors in superconducting magnets with applications to the CERN Large Hadron Collider," *Phys. Rev. ST Accel. Beams* vol. 3, 122403, December 2000.
[6] B. Bellesia, *et al.*, "Field quality in low-β superconducting quadrupoles and impact on the beam dynamics for the Large Hadron Collider upgrade," *Phys. Rev. ST Accel. Beams* vol. 10, 062401, June 2007.
[7] F. Borgnolutti *et al*., " Reproducibility of the Coil Positioning in Nb_3Sn Magnet Models Through Magnetic Measurements," *IEEE Trans. App. Supercond*, vol. 19, no. 3, pp. 1100-1105, July 2009.
[8] Original LARP Proposal, 2003, http://www.uslarp.org/LARP_Proposal.pdf
[9] F. Borgnolutti, *et al*., "Fabrication of a Second-Generation of Nb_3Sn Coils for the LARP HQ02 Quadrupole Magnet," *IEEE Trans. App. Supercond.*, vol. 24, no. 3, p. 4003005, June 2014.
[10] G. Chlachidze, *et al*., "Performance of HQ02, an Optimized Version of the 120 mm Nb_3Sn LARP Quadrupole", *IEEE Trans. App. Supercond.*, vol. 24, no. 3, pp.1-5, June 2014.
[11] S. Caspi, *et al.*, "Design of a 120 mm Bore 15 T Quadrupole for the LHC Upgrade Phase II," *IEEE Trans. Appl. Supercond*., vol. 20, no. 3, pp. 144-147, June 2010.
[12] J. DiMarco, *et al*., "Field Quality Measurements of LARP Nb3Sn Magnet HQ02," *IEEE Trans. App. Supercond*., vol. 24, no. 3, p4003905, June 2014.
[13] H. Bajas, *et al*., "Test Results of the LARP HQ02b Magnet at 1.9 K," *IEEE Trans. App. Supercond.*, vol. 24, no. 3, pp.1-5, June 2014.
[14] E.F. Holik *et al*., "Fabrication and Analysis of 150-mm-Aperture Nb_3Sn MQXF Coils," *IEEE Trans. App. Supercond*, vol. 26, no. 4, pp. 1-7, June 2016.
[15] F. Borgnolutti, *et al*., "Fabrication of a Third Generation of Nb_3Sn Coils for the LARP HQ03 Quadrupole Magnet," *IEEE Trans. App. Supercond*., vol. 24, no. 3, p. 4002505, June 2014.
[16] I. Rodriguez and J.L. Munoz, "Benchmark of COMSOL vs. ROXIE Codes for the Calculation of a Particle Accelerator Quadrupole," Excerpt from the Proceedings of the 2011 COMSOL Converence3 in Stuttgart, https://www.comsol.com/paper/download/83731/rodriguez_paper.pdf Downloaded August 2016.-